ELSEVIER

Soil Dynamics and Earthquake Engineering 22 (2002) 259–271

SOIL DYNAMICS AND EARTHQUAKE ENGINEERING

www.elsevier.com/locate/soildyn

Computational modeling of cyclic mobility and post-liquefaction site response

Ahmed Elgamal[a,*], Zhaohui Yang[a], Ender Parra[b]

[a]*Department of Structural Engineering, University of California, San Diego, La Jolla, CA 92093, USA*
[b]*PDVSA, INTEVEP, Urbanización Santa Rosa, Los Teques, P.O. Box 76343A, Caracas 1070A, Venezuela*

Received 29 January 2002; accepted 26 March 2002

Abstract

Under seismic excitation, liquefied clean medium to dense cohesionless soils may regain a high level of shear resistance at large shear strain excursions. This pattern of response, known as a form of cyclic mobility, has been documented by a large body of laboratory sample tests and centrifuge experiments. A plasticity-based constitutive model is developed with emphasis on simulating the cyclic mobility response mechanism and associated pattern of shear strain accumulation. This constitutive model is incorporated into a two-phase (solid–fluid), fully coupled finite element code. Calibration of the constitutive model is described, based on a unique set of laboratory triaxial tests (monotonic and cyclic) and dynamic centrifuge experiments. In this experimental series, Nevada sand at a relative density of about 40% is employed. The calibration effort focused on reproducing the salient characteristics of dynamic site response as dictated by the cyclic mobility mechanism. Finally, using the calibrated model, a numerical simulation is conducted to highlight the effect of excitation frequency content on post-liquefaction ground deformations. © 2002 Published by Elsevier Science Ltd.

Keywords: Liquefaction; Cyclic mobility; Constitutive modeling; Earthquake; Plasticity; Site amplification; Vertical array

1. Introduction

Liquefaction and associated shear deformations continue to cause extensive damage during strong earthquakes [1–11] (see also http://peer.berkeley.edu/turkey/adapazari). In clean medium to dense sands, the mechanism of liquefaction-induced shear deformation may be illustrated by the response depicted in Fig. 1 [12]. The simple shear test of Fig. 1 shows: (i) a cycle-by-cycle degradation in shear strength as manifested by the occurrence of increasingly larger shear strain excursions for the same level of applied shear stress, and (ii) a regain in shear stiffness and strength at these large shear strain excursions, along with an increase in effective confinement (shear-induced dilative tendency). This type of response has been described as a form of cyclic mobility in a large number of pioneering liquefaction studies [13–17]. Casagrande [15] indicates that when subjected to cyclic loading, sands with relative densities D_r of about 40% or above may develop cyclic mobility with strains of objectionable amplitude (Fig. 1), but rarely undergo actual liquefaction (i.e. flow-failure or unbounded shear deformation). Indeed, the response mechanism shown in Fig. 1 is representative of a large number of undrained laboratory experiments on medium–dense Nevada sand with D_r of about 40% and above [12].

For the important situations of lateral spreading or biased strain accumulation due to a superposed static shear stress (e.g. embankment slopes, below foundations, behind retaining walls, etc.), cyclic mobility may continue to play a dominant role [18–20]. This is clearly seen from the results of a triaxial test (Fig. 2, [12]), where a superposed driving shear stress causes the strain to occur in a biased (downslope) direction, on a cycle-by-cycle basis. Inspection of Fig. 2 shows that a net finite increment of permanent shear strain occurs in each cycle. Realistic estimation of the magnitude of such increments is among the most important considerations in assessments of liquefaction-induced hazards.

The above mentioned effects (Figs. 1 and 2) are thoroughly documented by a large body of experimental research worldwide (employing clean sands and clean nonplastic silts) including centrifuge experiments, shake-table tests, and cyclic laboratory sample tests [21]. In the project VELACS [22,23] (see also http://geoinfo.usc.edu/gees/velacs), extensive data sets were generated consistently revealing the cyclic mobility response characteristics. This data included results from a large number of laboratory

* Corresponding author. Fax: +1-858-822-2260.
E-mail address: elgamal@ucsd.edu (A. Elgamal).

0267-7261/02/$ - see front matter © 2002 Published by Elsevier Science Ltd.
PII: S0267-7261(02)00022-2

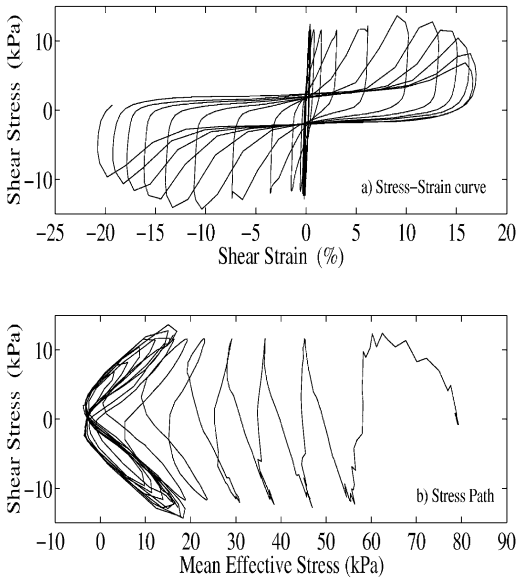

Fig. 1. Stress–strain and stress path response for Nevada sand ($D_r = 60\%$) in a stress-controlled, undrained cyclic simple shear test [12].

tests and dynamic centrifuge experiments, in which Nevada no. 120 sand was employed.

In light of the documented significance of cyclic mobility, a plasticity-based constitutive model was developed to reproduce the associated salient response characteristics [24–26]. This model was also incorporated into a solid–fluid fully coupled finite element (FE) code [25,26]. Model calibration was based on a selected set of the VELACS data (for Nevada sand at about 40% D_r), including (i) a series of monotonic and cyclic laboratory tests, and (ii) level-ground and infinite-slope centrifuge model simulations conducted at Rensselaer Polytechnic Institute (RPI)

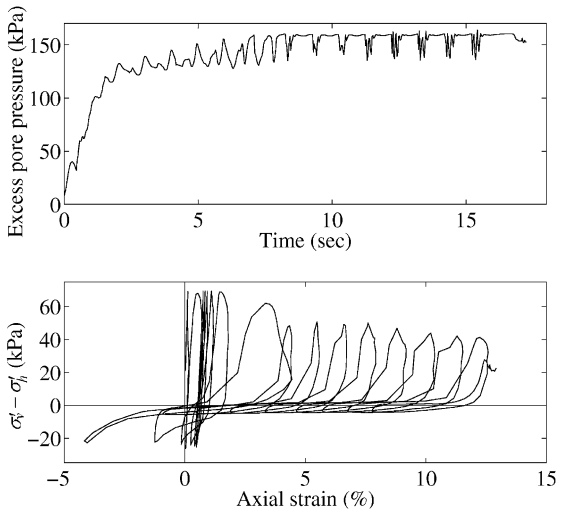

Fig. 2. Stress–strain and excess-pore-pressure histories during an undrained, anisotropically consolidated cyclic triaxial test of Nevada sand at $D_r = 40\%$ [12]. (σ'_v and σ'_h are vertical and horizontal effective stresses, respectively.)

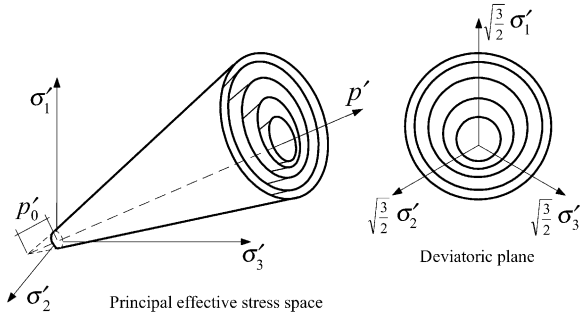

Fig. 3. Conical yield surface in principal stress space and deviatoric plane [30,24].

[18,27]. Our calibration effort attempted to obtain a satisfactory overall match of the entire employed data set.

In this paper, salient features of the constitutive model and the FE formulation are presented. Thereafter, the numerical calibration procedures and results are described and discussed. In addition, the calibrated FE code is employed to highlight the influence of input excitation frequency content on potential post-liquefaction shear deformations.

2. Constitutive model

A number of constitutive models have been developed to simulate cyclic-mobility and/or flow-liquefaction soil response [28–48]. Currently, reliable computational modeling of the cyclic-mobility effects on lateral spreading (Fig. 2) still remains a major challenge. Such situations necessitate a high degree of control over the accumulated cycle-by-cycle shear deformations. The developed constitutive model [24–26] is based on the framework of multi-surface plasticity [30,49,50], in which the salient cyclic-mobility response characteristics of Figs. 1 and 2 are reproduced by specifying a new appropriate flow rule. The main components of this model are summarized later (see Refs. [24–26] for more details).

2.1. Yield function

Following the classical plasticity convention [51], it is assumed that material elasticity is linear and isotropic, and that nonlinearity and anisotropy result from plasticity. The selected yield function [30] forms a conical surface in stress space with its apex along the hydrostatic axis (Fig. 3). In the context of multi-surface plasticity [30,49,50], a number of similar yield surfaces with a common apex and different sizes form the hardening zone (Fig. 3). The outmost surface is the envelope of peak shear strength (failure envelope).

2.2. Hardening rule

A purely deviatoric kinematic hardening rule [25,26] is employed in order to generate hysteretic response under

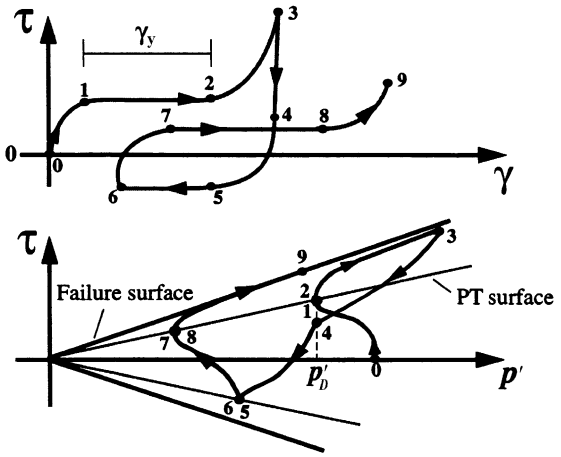

Fig. 4. Schematic of constitutive model response showing confinement-dependent yield surface for granular soils, shear stress–shear strain relationship, and shear stress–effective confinement relationship for undrained loading [24].

arbitrary cyclic shear loading. This rule was modified from the original Mroz rule [50], for improved numerical robustness. Kinematic hardening dictates that yield surfaces translate in stress space within the failure envelope [51].

2.3. Flow rule

In granular materials, shear loading induces a coupled volumetric response (contraction or dilation). The boundary between contraction and dilation is commonly defined by the phase transformation (PT) surface [52–55] in the deviatoric stress τ–effective confinement p' space (Fig. 4). As shear stress increases, soil volumetric response changes from contraction (below the PT surface) to dilation (above the PT surface). Under undrained conditions, the adopted flow rule defines the following phases of soil response [24–26]:

1. The contractive phase within the PT surface (Fig. 4, phase 0–1).
2. The dilative phase during shear loading, with the stress state outside the PT surface (Fig. 4, phase 2–3).
3. The contractive phase during shear unloading (Fig. 4, phase 3–4), until the effective confinement returns to p'_D.
4. The liquefaction-induced perfectly plastic phase during shear loading (Fig. 4, phase 1–2), before the initiation of dilation (Fig. 4, phase 2–3). This phase is significant only at very low confinement (e.g. below 10 kPa for Nevada sand), where considerable permanent shear strain (γ_y) may accumulate with minimal change in shear stress.

In summary, the main modeling parameters include (Table 1) standard dynamic soil properties such as low-strain shear modulus and friction angle, as well as calibration constants to control the dilatancy effects (PT angle, contraction and dilation parameters), and the level of liquefaction-induced yield strain (γ_y). Calibration procedures for these parameters are described later.

3. Finite element formulation

In order to study the dynamic response of saturated soil systems as an initial-boundary-value problem, a two-dimensiona plane-strain FE code was developed [25,26]. In this code, saturated soil is modeled as a two-phase material based on the Biot [56] theory for porous media. A simplified numerical framework of this theory, known as u–p formulation (in which displacement of the soil skeleton u, and pore pressure p, are the primary unknowns [57,58]), was implemented [25,26,59].

The u–p formulation is defined by [57] (i) the equation of motion for the solid–fluid mixture, and (ii) the equation of mass conservation for the fluid phase, incorporating equation of motion for the fluid phase and Darcy's law. These two governing equations may be expressed in the following FE matrix form [57]:

$$\mathbf{M}\ddot{\mathbf{U}} + \int_{\Omega} \mathbf{B}^{\mathrm{T}}\boldsymbol{\sigma}' \mathrm{d}\boldsymbol{\Omega} + \mathbf{Q}\mathbf{p} - \mathbf{f}^{\mathrm{s}} = 0 \tag{1a}$$

$$\mathbf{Q}^{\mathrm{T}}\dot{\mathbf{U}} + \mathbf{S}\dot{\mathbf{p}} + \mathbf{H}\mathbf{p} - \mathbf{f}^{\mathrm{p}} = 0 \tag{1b}$$

where $\mathbf{M}$ is the mass matrix, $\mathbf{U}$ the displacement vector, $\mathbf{B}$ the strain–displacement matrix, $\boldsymbol{\sigma}'$ the effective stress vector (determined by the soil constitutive model discussed earlier), $\mathbf{Q}$ the discrete gradient operator coupling the solid and fluid phases, $\mathbf{p}$ the pore pressure vector, $\mathbf{H}$ the permeability matrix,

Table 1
Model parameters [26] calibrated for $D_r = 40\%$ Nevada sand

Main calibration experiment	Parameter	Value
Drained monotonic tests	Low-strain shear modulus G_r (at 80 kPa mean effective confinement)	33.3 MPa
	Friction angle ϕ	31.4°
Undrained cyclic test	Liquefaction yield strain γ_y (Fig. 4, phase 1–2)	1.0%
RPI centrifuge Model 1	Contraction parameter c_1	0.17
	Contraction parameter c_2 (Fig. 4, phase 0–1)	0.05
RPI centrifuge Model 2	Phase transformation angle ϕ_{PT}	26.5°
	Dilation parameter d_1	0.4
	Dilation parameter d_2 (Fig. 4, phase 2–3)	100.0

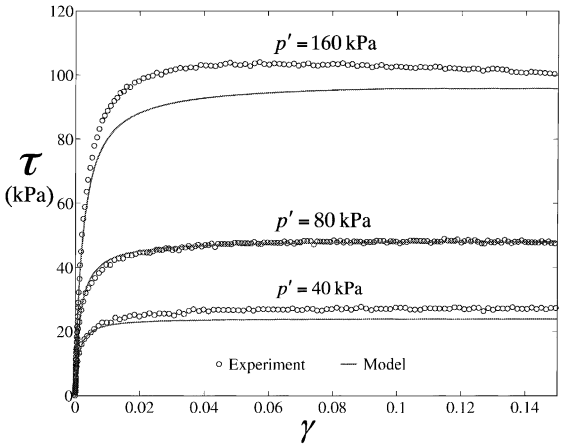

Fig. 5. Octahedral shear stress–strain curves for Nevada sand at 40% D_r from isotropically consolidated drained triaxial tests [12,26].

S the compressibility matrix, a superposed T denotes matrix transpose, and a superposed dot denotes time derivative. The vectors $\mathbf{f}^s$ and $\mathbf{f}^p$ include the effects of body forces and prescribed boundary conditions for the solid–fluid mixture and the fluid phase, respectively. In Eq. (1a) (equation of motion), the first term represents inertia force of the mixture, followed by internal force due to soil skeleton deformation, and internal force induced by pore-fluid pressure. In Eq. (1b) (mass conservation), the first two terms represent the rate of volume change for the soil skeleton and the fluid phase, respectively, followed by seepage rate of the pore fluid.

4. Model calibration

The calibration procedure was carried out for Nevada sand at about 40% D_r, with emphasis on reproducing the observed cycle-by-cycle accumulation of shear deformations (Figs. 1, 2, and 4). This calibration effort attempted to obtain a satisfactory overall match of the entire employed data set, including (refer to Table 1):

1. Data of a drained monotonic triaxial test [12] employed to define the low-strain shear modulus and the friction angle.
2. The liquefaction-induced yield strain (γ_y) calibrated mainly based on matching the recorded response in an anisotropically consolidated, undrained cyclic triaxial test [12].
3. The pore-pressure buildup (contraction) parameters calibrated based on simulation of a dynamic centrifuge test of liquefying level ground [18,19], and
4. The PT angle and dilation parameters calibrated through simulations of a dynamic centrifuge test of a mildly inclined infinite slope [18,19]. This test also served as verification for the cyclic shear strain parameter calibrated in step 2 above.

In the following sections, each employed experimental phase is briefly described, along with the recorded responses and calibration results.

4.1. Drained monotonic triaxial test

A monotonic consolidated-isotropically, drained, compression (CIDC) triaxial test was conducted on Nevada sand at about 42% D_r [12]. In this test, the sample was first isotropically consolidated to $p' = 80$ kPa. Thereafter, the vertical pressure was gradually increased, with the lateral confining pressure simultaneously decreased, so that p' remained constant throughout the test. The (octahedral) shear stress–strain response recorded during this test (Fig. 5) was matched by the constitutive model, using a least-squares curve-fitting procedure [26]. This matching exercise defined the low-strain shear modulus and the friction angle (Table 1). Finally, it can be seen that (Fig. 5) the identified properties resulted in a reasonable match of two additional CIDC experiments conducted at $p' = 40$ kPa and 160 kPa, respectively [12].

4.2. Undrained cyclic triaxial test

An anisotropically consolidated, undrained cyclic triaxial test was conducted on Nevada sand at an initial D_r of about 39% [12]. The soil sample was first consolidated to a mean confinement $p' = 160$ kPa, with the vertical principal stress (σ'_v) greater than the horizontal components (σ'_h) by 20 kPa (anisotropic confinement or shear stress bias). Thereafter, the sample remained undrained, and a stress-controlled cyclic load was applied vertically.

The test was numerically simulated using the constitutive model (undrained condition was specified by prescribing a state of zero volumetric strain such that $\varepsilon_h = -\varepsilon_v/2$ [25,26]). In this test, the level of deformations was consistent with the centrifuge Model 2 experiment discussed later. Therefore, the parameter controlling the cycle-by-cycle accumulation of permanent strain (γ_y in Table 1) was calibrated by matching the last seven cycles of this triaxial test (Fig. 6). It may be noted that a sudden large pore pressure buildup occurred during the first two loading cycles of the test (Fig. 6). However, a second essentially identical triaxial test (Test No. 40-50 [12]) did not display similar behavior (i.e. pore pressure buildup was not consistent between these two experiments, making this part of the data unreliable). Thus, pore pressure development was based on the centrifuge data discussed later, which suggested the gradual buildup mechanism in the numerical response of Fig. 6.

4.3. Centrifuge experiments

In the VELACS project, two centrifuge model tests (Fig. 7) were conducted by Dobry and Taboada [60] to simulate the dynamic response of level and mildly sloping sand sites. Results of these two tests were employed for calibration of model contraction/dilation parameters, through FE simulations. The employed centrifuge

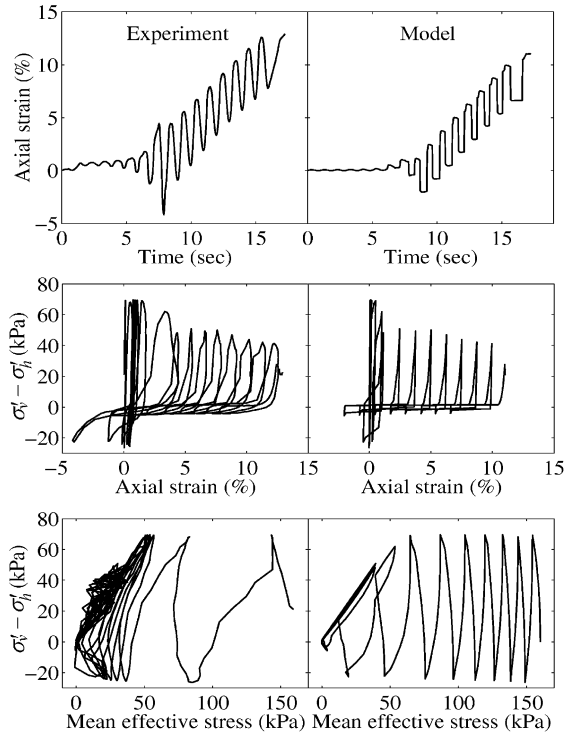

Fig. 6. Recorded and computed results of anisotropically consolidated, undrained cyclic triaxial test (Nevada sand at 40% D_r) with static stress bias [12,26].

models are [27]:

1. VELACS Model 1 representing a level site, subjected to a predominantly 2 Hz harmonic base excitation, and
2. VELACS Model 2 representing a mildly inclined infinite slope with an effective inclination angle of about 4°, subjected to a predominantly 2 Hz harmonic base excitation.

These tests were performed in a laminated container [61,62] that allows relative slip between laminates in order to simulate approximately one-dimensional (1D) shear response (Fig. 7). Nevada sand was used at D_r in the range of 40–45%. The soil models were spun to a 50g gravitational field [27]. At this gravitational field, the centrifuge models aim to simulate a prototype stratum of 10 m depth and infinite lateral extent. Water was used as the pore fluid, resulting in a prototype soil permeability equal to 50 times that of the model soil [63]. The results of these tests were thoroughly documented in Ref. [27], and further analyzed in Refs. [27,60,64].

4.4. Numerical modeling procedures

The centrifuge tests were simulated using the above-described FE procedure (Fig. 8). The boundary conditions were (i) dynamic excitation was defined as the recorded base acceleration, (ii) at any given depth, displacement degrees of freedom were tied together (both horizontally and vertically using the penalty method) to reproduce a 1D shear beam effect [25], (iii) the surface was traction free, with zero prescribed pore pressure, and (iv) the base and lateral boundaries were impervious.

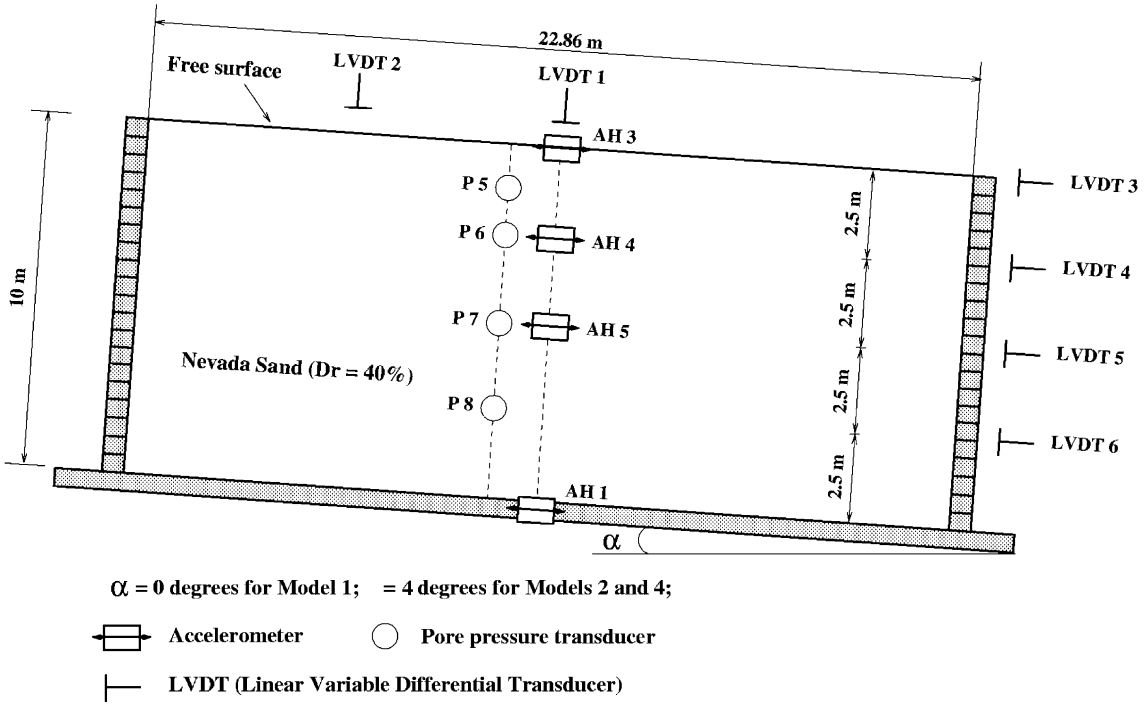

Fig. 7. General configurations of RPI centrifuge Models 1 and 2 in laminar container [27].

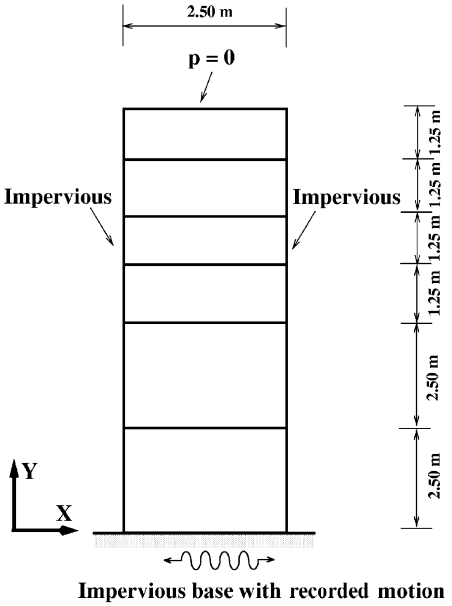

Fig. 8. Finite element discretization and boundary conditions.

A static application of gravity (model own weight) was performed before seismic excitation. The resulting fluid hydrostatic pressures and soil stress-states along the soil column served as initial conditions for the subsequent dynamic analysis.

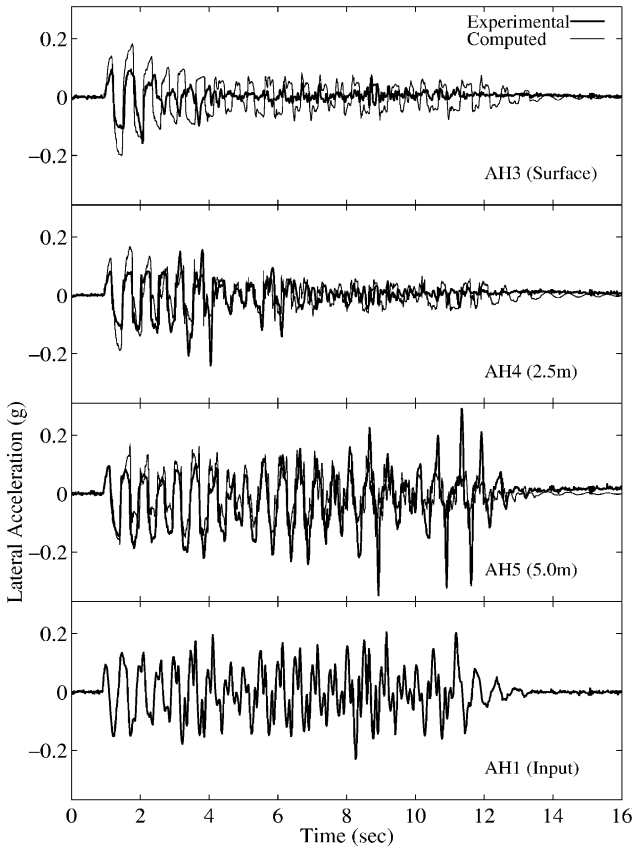

Fig. 9. Model 1 recorded and computed acceleration time histories.

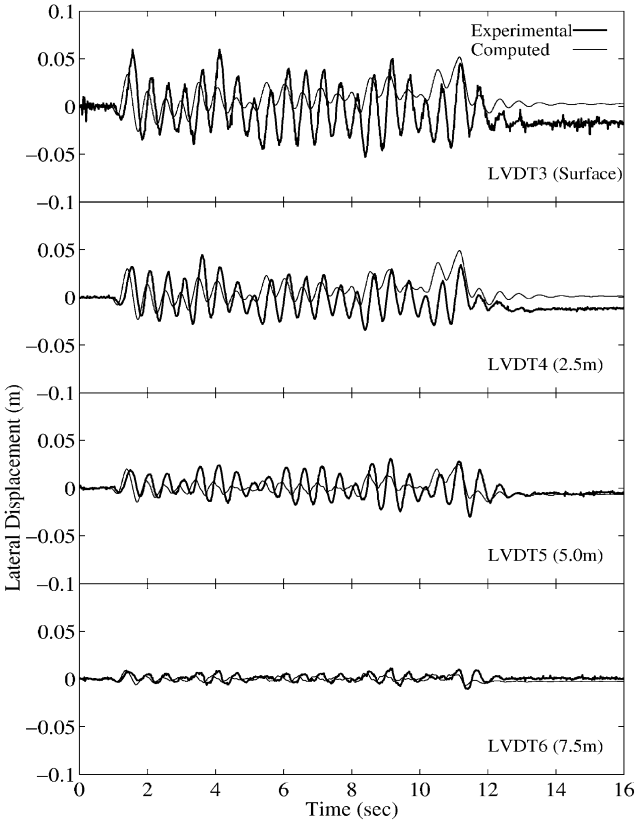

Fig. 10. Model 1 recorded and computed lateral displacement histories.

4.4.1. Level site: Model 1

Figs. 9–11 display the computed and recorded lateral accelerations, displacements, and pore-pressures. In general, good agreement was achieved between the computed and recorded responses. At the free surface, accelerations virtually disappeared after about 4 s due to liquefaction (AH3, Fig. 9). At 2.5 m depth, a similar mechanism followed after about 6 s (AH4, Fig. 9). Liquefaction was reached down to a depth of 5 m (Fig. 11), as indicated by the pore-pressure ratio r_u approaching 1.0 ($r_u = u_e/\sigma'_v$ where u_e is excess pore-pressure, and σ'_v initial effective vertical stress). The top sections of the model remained liquefied until the end of shaking and beyond. Thereafter, excess pore pressure started to dissipate.

Relatively small lateral displacements were observed in this case (Fig. 10). In fact, the cyclic shear strains were generally below 1% (Fig. 12). These stress–strain histories (Fig. 12) display the usual pattern of stiffness loss due to pore-pressure buildup (Fig. 11). Liquefaction at the 2.5–5.5 m depth zone appears to isolate the upper layers (surface to 1.5 m depth) from experiencing large strains.

The stress-paths of Fig. 13 show the typical mechanism of cyclic decrease in effective confinement due to pore-pressure buildup (Fig. 11). This data (Fig. 11) was a main source for calibration of model pore-pressure buildup (shear-induced contraction) parameters (c_1 and c_2 in Table 1). Overall, it may be noted that the relatively small strains

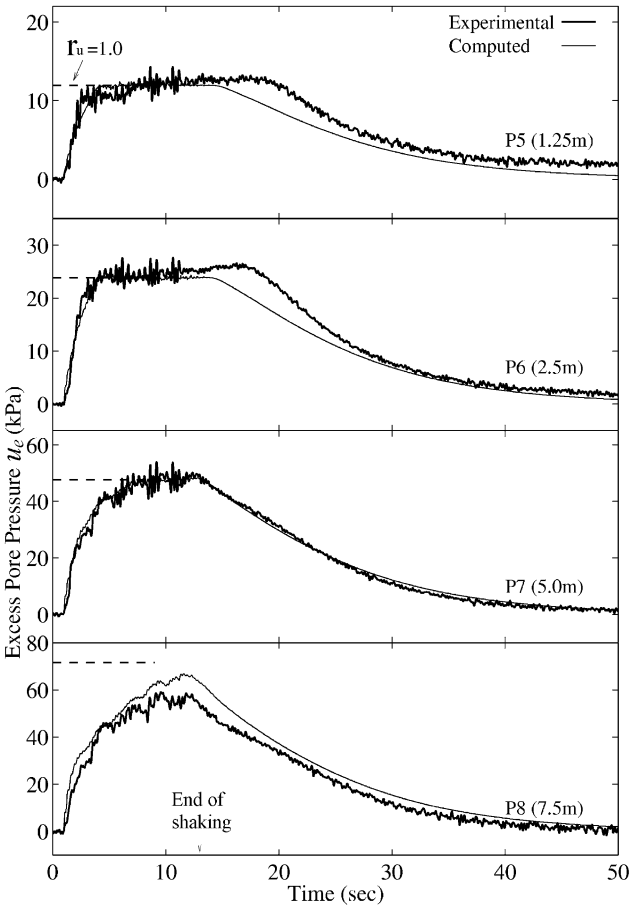

Fig. 11. Model 1 recorded and computed excess pore pressure time histories.

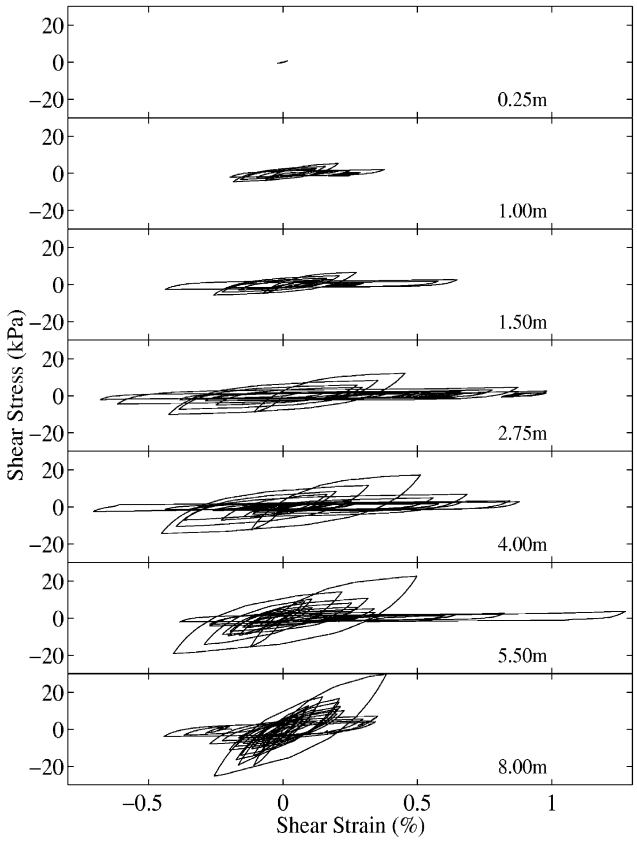

Fig. 12. Model 1 computed shear stress–strain histories.

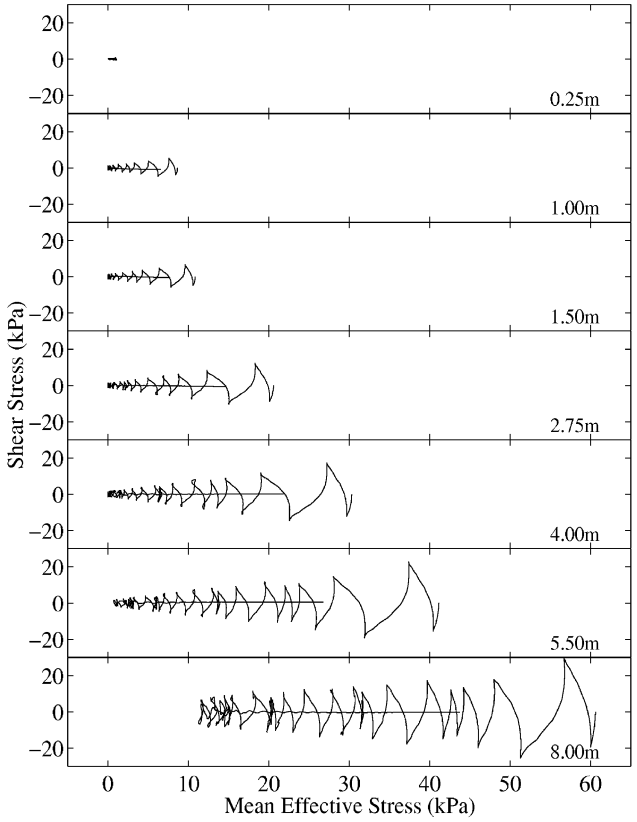

Fig. 13. Model 1 computed effective stress path.

during liquefaction (Fig. 12) led to soil response (Fig. 13) predominantly below the PT surface (i.e. virtual absence of dilative tendency). The infinite-slope model below displayed much larger accumulated strain levels and allowed for calibration of dilative model response above the PT surface.

4.4.2. Mild slope: Model 2

The 4° inclination of Model 2 imposed a static shear stress component (due to gravity), causing accumulated cycle-by-cycle lateral deformation. Despite the relatively mild inclination, all response characteristics (Figs. 14–16) are much different from those of Model 1 above (Figs. 9–11). Surface accelerations were sustained throughout the shaking phase (Fig. 14), and lateral displacements reached a permanent value of 0.5 m (Fig. 15). The recorded and computed u_e histories (Fig. 16) both displayed a number of instantaneous sharp pore pressure drops after initial liquefaction. These drops coincided with the observed and computed acceleration spikes that occurred exclusively in the negative direction (Fig. 14).

The cause of these observed asymmetric accelerations and sharp pore pressure drops may be inferred from the computed shear stress–strains (Fig. 17) and effective stress

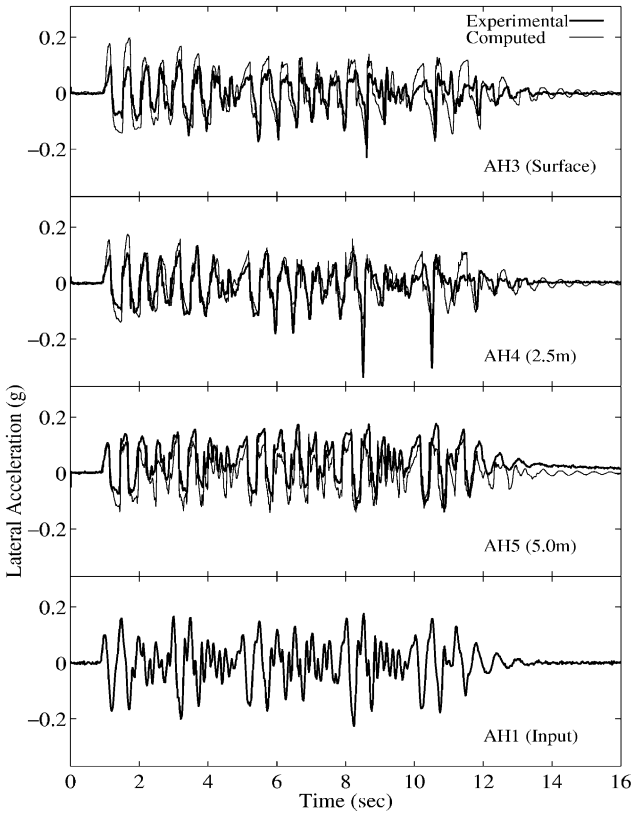

Fig. 14. Model 2 recorded and computed acceleration time histories.

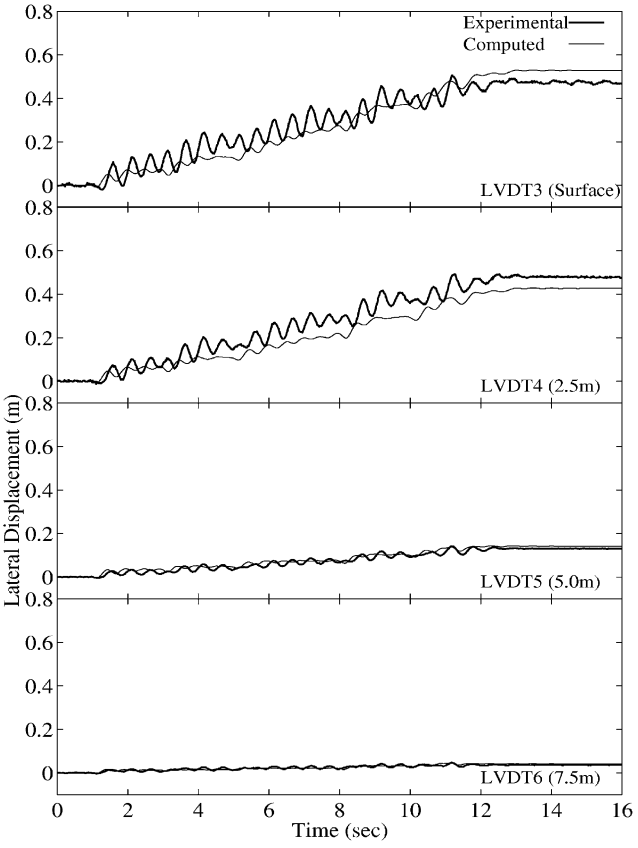

Fig. 15. Model 2 recorded and computed lateral displacement histories.

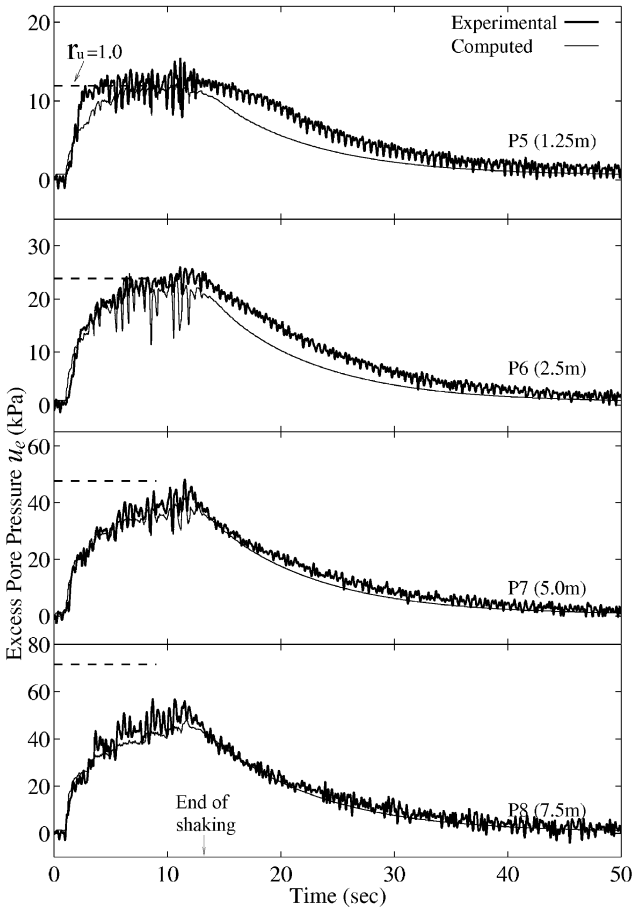

Fig. 16. Model 2 recorded and computed excess pore pressure time histories.

paths (Fig. 18). In these figures, the presence of dilative response prevailed, in terms of instantaneous regain in effective confinement and shear strength at large strains. This response characteristic was especially evident in the upper sections after initial liquefaction ($r_u = 1$). Thus, dilation-induced regain in shear strength appears to be the main cause of the large acceleration spikes after liquefaction. The responses of Figs. 17 and 18 manifest the role of Model 2 in calibrating the constitutive model response above the PT surface (PT angle and dilation parameters d_1 and d_2 in Table 1). In addition, reasonably good agreement between the computed and recorded lateral displacements along the soil column verified the calibrated yield strain γ_y (Table 1), an important parameter in dictating the extent of post-liquefaction cycle-by-cycle shear deformations.

Remark: The numerically predicted settlement due to liquefaction was generally smaller than observations. Indeed, Models 1 and 2 resulted in settlement in the range of 0.1–0.2 m (1–2% of layer thickness), which was considerably underpredicted (numerical estimate was 0.05 m). A highly nonlinear bulk modulus may be needed to simulate such post-liquefaction densification-induced settlements (a topic of current ongoing research).

The undertaken model calibration phase is now complete.

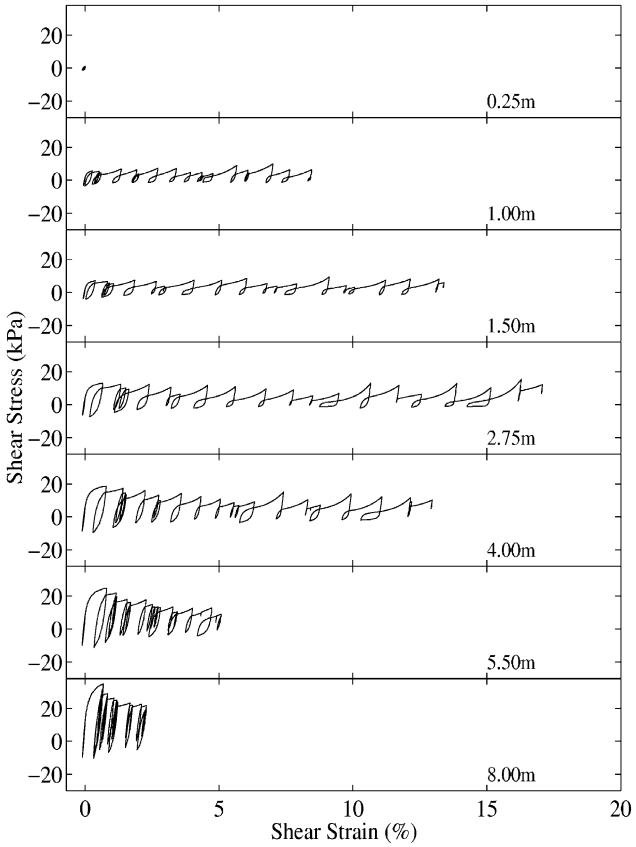

Fig. 17. Model 2 computed shear stress–strain histories.

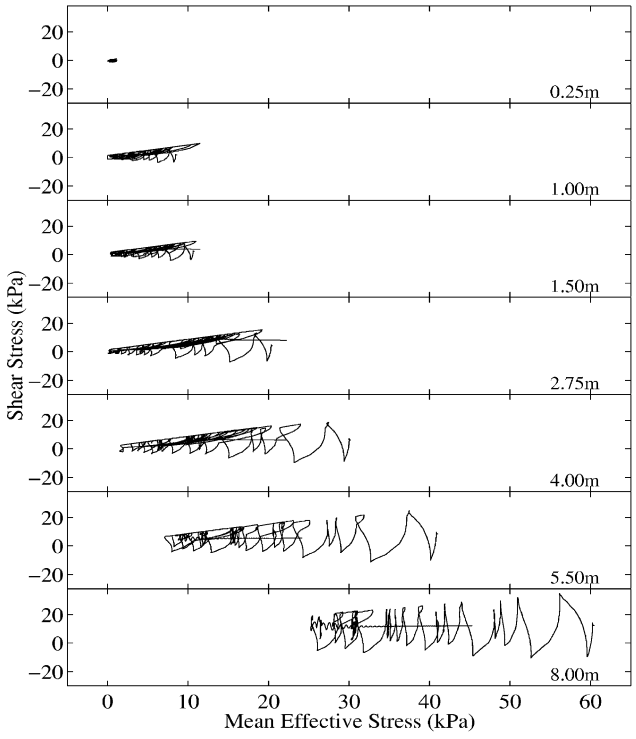

Fig. 18. Model 2 computed effective stress path.

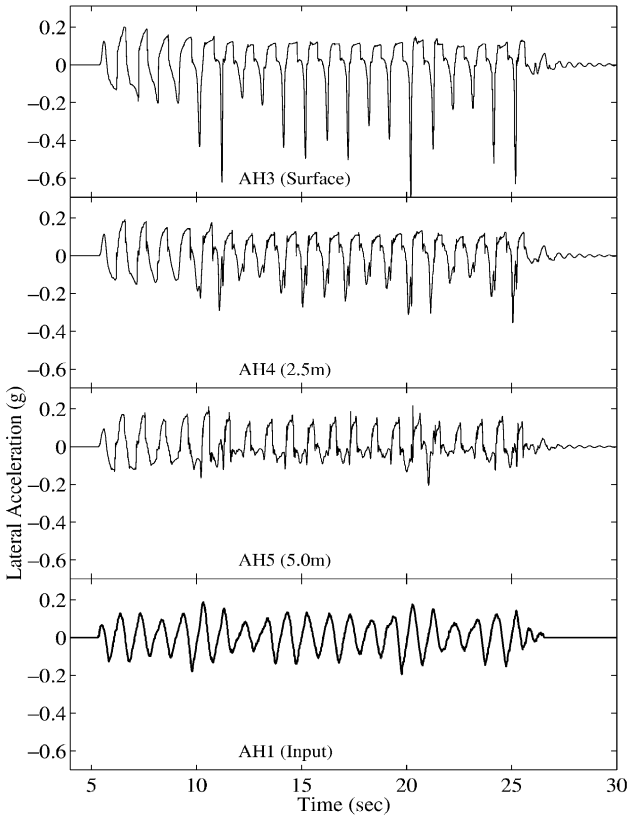

Fig. 19. Computed acceleration time histories (1.0 Hz case).

In the subsequent numerical simulation, shear deformation during liquefaction will evolve based on the calibrated model constants listed in Table 1.

5. Numerical simulation

In order to further appreciate the impact of dilation on liquefaction-induced shear deformation, an additional 1D numerical simulation was conducted with a base excitation of lower predominant frequency (1.0 Hz compared to 2.0 Hz in Model 2). Seismically, such low frequency excitation may be associated with large distant earthquakes. The model configuration and all other numerical simulation parameters were identical to Model 2 above.

The computed results are shown in Figs. 19–23. Once the soil liquefied, the relatively low shaking frequency allowed for larger shear deformations in each cycle of excitation (Figs. 20 and 22). These large cyclic shear strains in turn induced a significant dilative response above the PT surface (Fig. 23), causing the soil to regain much stiffness and strength in nearly all load cycles (Fig. 22). In addition, the following notable consequences are observed near ground surface: (i) asymmetric acceleration spikes (Fig. 19, reaching a peak of 0.6g, nearly three times the input), and (ii) significant instances of pore-pressure reduction (Fig. 21).

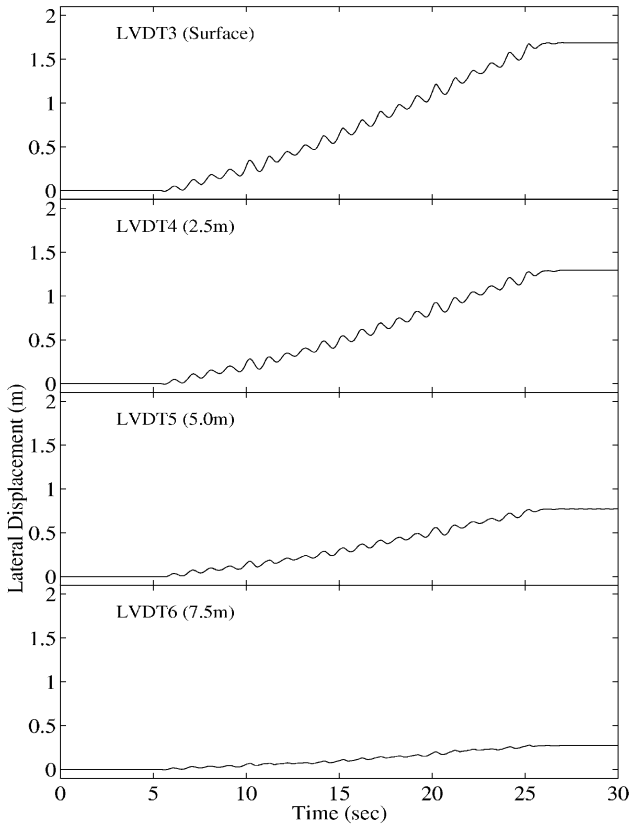

Fig. 20. Computed lateral displacement time histories (1.0 Hz case).

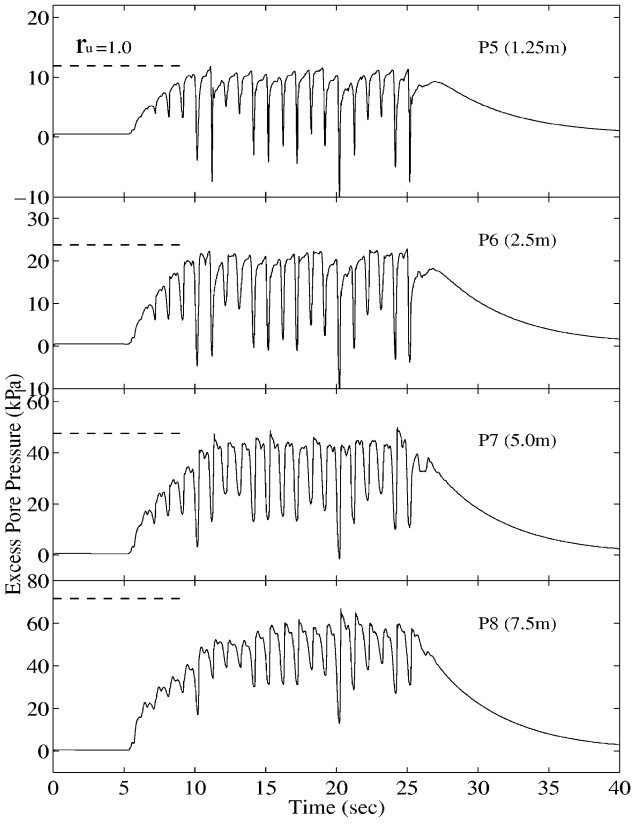

Fig. 21. Computed excess pore pressure time histories (1.0 Hz case).

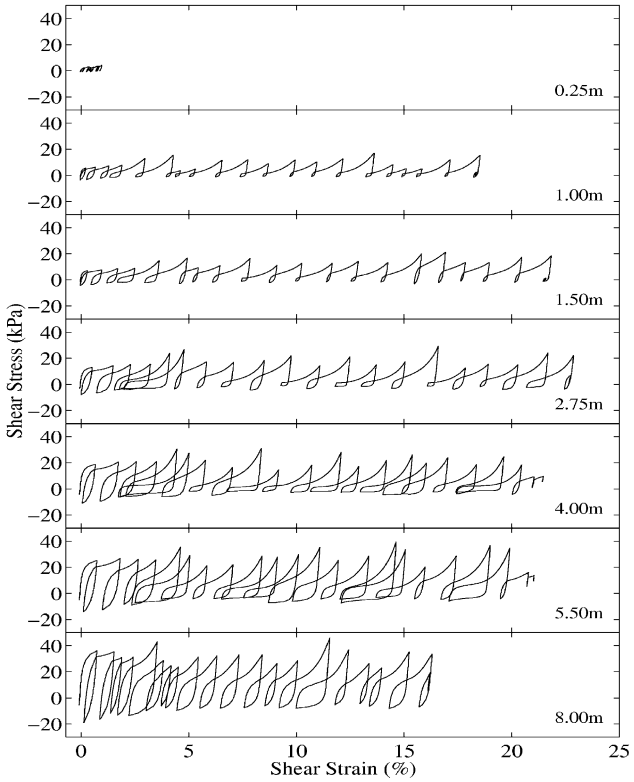

Fig. 22. Computed shear stress–strain histories (1.0 Hz case).

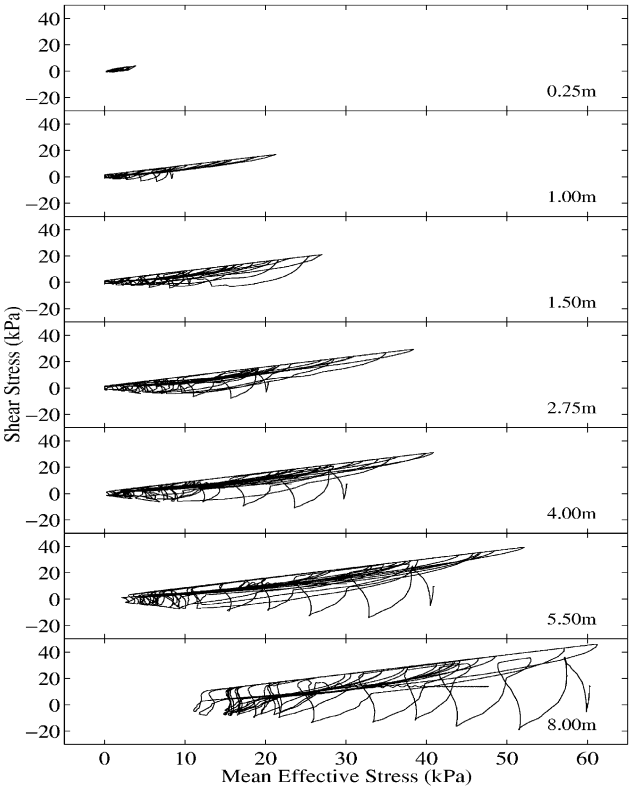

Fig. 23. Computed effective stress path (1.0 Hz case).

This numerical simulation suggests two important response characteristics. For a saturated medium to dense sand or similar soil formation, it may be seen that a lower predominant frequency of excitation may result in (i) much increased accumulation of permanent shear deformations (compare Figs. 15 and 20), and (ii) along with the pore pressure spikes, larger peak ground accelerations (compare Figs. 14 and 19).

6. Summary and conclusions

A constitutive model was developed for cyclic mobility analyses. The model was integrated into a solid–fluid fully coupled FE formulation. A large set of experimental data was used to calibrate the constitutive model and the associated FE framework. The calibration process was described with emphasis on reproducing the cyclic mobility effects associated with liquefaction-induced shear deformations in clean medium–dense granular soil profiles. Accuracy in predicting such deformations is of utmost practical significance in structural/foundation stability and damage assessments. Using the calibrated model, an additional simulation was conducted to illustrate the potential impact of frequency content on accumulated deformations, and on magnitude of ground surface acceleration.

For saturated medium–dense cohesionless soils, the presented dynamic excitation response showed that:

1. Under level ground conditions, shear strains were relatively small with minor cyclic mobility effects. This aspect was noted earlier in an analysis of the Port Island (1995 Kobe, Japan earthquake) liquefaction case history [65].
2. Mildly sloping ground may result in large cyclic shear strain accumulation. These large strains induce pronounced cyclic mobility effects (regain in shear resistance), and result in sharp surface acceleration spikes. In the presence of cyclic mobility, unbounded flow failure is unlikely to occur.
3. The dominant excitation frequency has a significant impact on post-liquefaction soil response. Low-frequency input excitation (e.g. due to very large distant earthquakes) may significantly increase lateral deformations and the level of acceleration amplification at ground surface.

Acknowledgements

This work was supported by the Earthquake Engineering Research Centers Program of the National Science Foundation under Award Number EEC-9701568. Financial support for this research is gratefully acknowledged. In addition, the authors are most grateful to Professor Ricardo Dobry (RPI) and Professor Victor Taboada (UNAM, Mexico) for sharing the centrifuge data (VELACS Models 1 and 2) and for many valuable discussions.

References

[1] Seed RB, Dickenson SE, Riemer MF, Bray JD, Sitar N, Mitchell JK, Idriss IM, Kayen RE, Kropp A, Harder Jr LF, Power MS. Preliminary report on the principal geotechnical aspects of the October 17, 1989, Loma Prieta earthquake. Report no. UCB/EERC-90/05. Berkely, CA: Earthquake Engineering Research Center, 1990.

[2] Bardet JP, Oka F, Sugito M, Yashima A. The great Hanshin earthquake disaster. Preliminary investigation report. Los Angeles, CA: University of Southern California, 1995.

[3] Geotechnical reconnaissance of the effects of the January 17, 1995. In: Sitar N, editor. Report no. UCB/EERC-95/01, Berkeley, CA: Earthquake Engineering Research Center, 1995.

[4] Yegian MK, Ghahraman VG, Nogole-Sadat MAA, Daraie H. Liquefaction during the 1990 Manjil, Iran, earthquake. I. Case history data. Bull Seismol Soc Am 1995;85:66–82.

[5] Yegian MK, Ghahraman VG, Nogole-Sadat MAA, Daraie H. Liquefaction during the 1990 Manjil, Iran, earthquake. I. Case history data. Bull Seismol Soc Am 1995;85:83–92.

[6] Tuttle M, Barstow N. Liquefaction-related ground failure: a case study in the New Madrid seismic zone, Central United States. Bull Seismol Soc Am 1996;86:636–45.

[7] Japanese Geotechnical Society. Special issue on geotechnical aspects of the January 17, 1995 Hyogoken-Nanbu earthquake. Soils Found J (Tokyo, Japan) 1996.

[8] Japanese Geotechnical Society. Special issue on geotechnical aspects of the January 17, 1995 Hyogoken-Nanbu earthquake, no. 2. Soils Found J (Tokyo, Japan) 1998.

[9] Finn WDL. Seismic safety of embankment dams: developments in research and practice 1988–1998. In: Dakoulas P, Yegian M, Holtz B, editors. Geotechnical earthquake engineering and soil dynamics III, August 3–6, Seattle, WA, ASCE Geotechnical Special Publication No. 75, vol. 2. 1998. p. 812–53 invited paper.

[10] O'Rourke TD, Bardet JP, Hamada M, editors. Proceedings of the Seventh U.S.–Japan Workshop on Earthquake Resistant Design of Lifeline Facilities and Countermeasures against Soil Liquefaction. Technical Report MCEER-99-0019. Buffalo, NY, 1999.

[11] Archuleta RJ, Bonilla LF, Lavallee D. Nonlinearity in observed and computed accelerograms (CD-ROM). Proceedings of the 12th World Conference on Earthquake Engineering. Paper No. 1934. Auckland, New Zealand, 2000.

[12] Arulmoli K, Muraleetharan KK, Hossain MM, Fruth LS. VELACS: verification of liquefaction analyses by centrifuge studies, laboratory testing program, soil data report, Project no. 90-0562. Irvine, CA: Earth Technology Corp, 1992.

[13] Seed HB, Lee KL. Liquefaction of saturated sands during cyclic loading. J Soil Mech Found Div, ASCE 1966;92(SM6):105–34.

[14] Castro G. Liquefaction of sands, Harvard soil mechanics series 87. Cambridge, MA: Harvard University, 1969.

[15] Casagrande A. Liquefaction and cyclic deformation of sands—a critical review. Proceedings of the Fifth Pan-American Conference on Soil Mechanics and Foundation Engineering, Buenos Aires, Argentina, 1975.

[16] Castro G, Poulos SJ. Factors affecting liquefaction and cyclic mobility. J Geotech Eng Div, ASCE 1977;103(GT6):501–16.

[17] Seed HB. Soil liquefaction and cyclic mobility evaluation for level ground during earthquakes. J Geotech Eng Div, ASCE 1979; 105(GT2):201–55.

[18] Dobry R, Taboada V, Liu L. Centrifuge modeling of liquefaction effects during earthquakes. Proceedings of the First International Conference on Earthquake Geotechnical Engineering. Tokyo, Japan, 1995. p. 1291–324.

[19] Dobry R, Abdoun T. Post-triggering response of liquefied sand in the free field and near foundations. In: Dakoulas P, Yegian M, Holtz RD, editors. Proceedings, Geotechnical Earthquake Engineering and Soil Dynamics III, Aug 3–6, Seattle, WA, ASCE Geotechnical Special Publication No. 75, vol. 2. 1998. p. 270–300.

[20] Balakrishnan A, Kutter BL. Settlement, sliding and liquefaction of layered soil. J Geotech Geoenv Eng, ASCE 1999;125(11):968–78.

[21] Elgamal AW, Dobry R, Parra E, Yang Z. Soil dilation and shear deformations during liquefaction. In: Prakash S, editor. Proceedingsof the Fourth International Conference on Case Histories in Geotechnical Engineering. March 8–15, St Louis, MO, 1998. p. 1238–59.

[22] Arulanandan K, Scott RF, editors. Verification of numerical procedures for the analysis of soil liquefaction problems, vol. 1. Rotterdam: Balkema, 1993.

[23] Arulanandan K, Scott RF, editors. Verification of numerical procedures for the analysis of soil liquefaction problems, vol. 2. Rotterdam: Balkema, 1994.

[24] Elgamal A, Lai T, Yang Z, He L. Dynamic soil properties, seismic downhole arrays and applications in practice (CD-ROM). State-of-the-art paper. In: Prakash S, editor. Proceedings of the Fourth International Conference on Recent Advances in Geotechnical Earthquake Engineering and Soil Dynamics, March 26–31, San Diego, CA, 2001.

[25] Parra E. Numerical modeling of liquefaction and lateral ground deformation including cyclic mobility and dilation response in soil systems. PhD Thesis, Department of Civil Engineering, Rensselaer Polytechnic Institute, Troy, NY, 1996.

[26] Yang Z. Numerical modeling of earthquake site response including dilation and liquefaction. PhD Dissertation, Department of Civil Engineering and Engineering Mechanics, Columbia University, New York, NY, 2000.

[27] Taboada VM. Centrifuge modeling of earthquake-induced lateral spreading in sand using a laminar box. PhD Thesis, Rensselaer Polytechnic Institute, Troy, NY, 1995.

[28] Finn WDL, Lee KW, Martin GR. An effective stress model for liquefaction. J Geotech Eng Div, ASCE 1977;103:513–33.

[29] Nemat-Nasser S, Shokooh A. A unified approach to densification and liquefaction of cohesionless sand in cyclic shearing. Can Geotech J 1979;16:659–78.

[30] Prevost JH. A simple plasticity theory for frictional cohesionless soils. Soil Dyn Earthquake Eng 1985;4(1):9–17.

[31] Pastor M, Zienkiewicz OC. A generalized plasticity hierarchical model for sand under monotonic and cyclic loading. In: Pande GN, Van Impe WF, editors. Proceedings of the Second International Conference on Numerical Models in Geomechanics, 1986. p. 131–50.

[32] Wang ZL, Dafalias YF, Shen CK. Bounding surface hypoplasticity model for sand. J Eng Mech, ASCE 1990;116:983–1001.

[33] Iai S. A strain space multiple mechanism model for cyclic behavior of sand and its application, Earthquake engineering research note no. 43. Japan: Port and Harbor Research Institute, Ministry of Transport, 1991.

[34] Proubet J. Application of computational geomechanics to description of soil behavior. PhD Dissertation, University of Southern California, Los Angeles, CA, 1991.

[35] Anandarajah A. VELACS project: elasto-plastic finite element predictions of the liquefaction behavior of centrifuge models no. 1, 3 and 4a. In: Arulanandan K, Scott RF, editors. Proceedings of the International Conference on the Verification of Numerical Procedures for the Analysis of Soil Liquefaction Problems, vol. 1. Rotterdam: Balkema, 1993. p. 45–66.

[36] Aubry D, Benzenati I, Modaressi A. Numerical predictions for model no. 1. In: Arulanandan K, Scott RF, editors. Proceedings of the International Conference on the Verification of Numerical Procedures for the Analysis of Soil Liquefaction Problems, vol. 1. Rotterdam: Balkema, 1993. p. 45–66.

[37] Bardet JP, Huang Q, Chi SW. Numerical prediction for model no. 1. In: Arulanandan K, Scott RF, editors. Proceedings of the International Conference on the Verification of Numerical Procedures for the Analysis of Soil Liquefaction Problems, vol. 1. Rotterdam: Balkema, 1993. p. 67–86.

[38] Oka F, Yashima A, Shibata T, Kato M, Uzuoka R. FEM–FDM coupled liquefaction analysis of a porous soil using an elasto-plastic model. Appl Scient Res 1994;52:209–45.

[39] Muraleetharan KK, Mish KD, Arulanandan K. A fully coupled nonlinear dynamic analysis procedure and its verification using centrifuge test results. Int J Numer Anal Methods Geomech 1994; 18:305–25.

[40] Byrne PM, McIntyre J. Deformations in granular soils due to cyclic loading, Proceedings of Settlement 94, Texas. ASCE Geotechnical Special Publication No. 40 1994 p. 1864–96.

[41] Tateishi A, Taguchi Y, Oka F, Yashima A. A cyclic elasto-plastic model for sand and its application under various stress conditions, Proceedings of the First International Conference on Earthquake Geotechnical Engineering, vol. 1. Rotterdam: Balkema, 1995 pp. 399–404.

[42] Manzari MT, Dafalias YF. A critical state two-surface plasticity model for sands. Geotechnique 1997;49(2):252–72.

[43] Cubrinovski M, Ishihara K. State concept and modified elasto-plasticity for sand modeling. Soils Found 1998;38(4):213–25.

[44] Dafalias YF, Manzari MT. Modeling of fabric effect on the cyclic loading response of granular soils. In: Jones N, Ghanem R, editors. Proceedings of ASCE 13th Engineering Mechanics Conference, 13–16 June, Baltimore, MD, 1999.

[45] Borja RI, Chao HY, Montans F, Lin CH. Nonlinear ground response at Lotung LSST site. J Geotech Geoenv Eng, ASCE 1999;125(3): 187–97.

[46] Li XS, Dafalias YF. Dilatancy for cohesionless soils. Geotechnique 2000;50(4):449–60.

[47] Archuleta RJ, Lavallee D, Bonilla LF. New observations and methods for modeling nonlinear site response (CD-ROM). Proceedings of the Fourth International Conference on Recent Advances in Geotechnical Earthquake Engineering and Soil Dynamics and Symposium in Honor of Professor W.D. Liam Finn, March 26–31, San Diego, CA, Paper No. 3.13, 2001.

[48] Arduino P, Kramer S, Baska D. UW-sand: a simple constitutive model for liquefiable soils. 2001 Mechanics and Materials Summer Conference, June 27–29, San Diego, CA, 2001.

[49] Iwan WD. On a class of models for the yielding behavior of continuous and composite systems. J Appl Mech, ASME 1967;34:612–7.

[50] Mroz Z. On the description of anisotropic work hardening. J Mech Phys Solids 1967;15:163–75.

[51] Hill R. The mathematical theory of plasticity. London: Oxford University Press, 1950.

[52] Ishihara K. Stability of natural deposits during earthquakes. Theme Lecture. Proceedings of the 11th International Conference on Soil Mechanics and Foundation Engineering, San Francisco, CA, vol. 2, 1985. p. 321–76.

[53] Vaid YP, Thomas J. Liquefaction and postliquefaction behavior of sand. J Geotech Eng, ASCE 1995;121(2):163–73.

[54] Kramer SL. Geotechnical earthquake engineering. Upper Saddle River: Prentice Hall, 1996.

[55] Vaid YP, Sivathayalan S. Fundamental factors affecting liquefaction susceptibility of sands. In: Lade P, Yamamuro J, editors. Physics and mechanics of soil liquefaction, Rotterdam: Balkema, 1999. p. 105–20.

[56] Biot MA. The mechanics of deformation and acoustic propagation in porous media. J Appl Phys 1962;33(4):1482–98.

[57] Chan AHC. A unified finite element solution to static and dynamic problems in geomechanics. PhD dissertation, University College of Swansea, UK, 1988.

[58] Zienkiewicz OC, Chan AHC, Pastor M, Paul DK, Shiomi T. Static and dynamic behavior of soils: a rational approach to quantitative solutions. I. Fully saturated problems. Proc R Soc Lond A 1990;429:285–309.

[59] Ragheb A. Numerical analysis of seismically induced deformations in

saturated granular soil strata. PhD Thesis, Rensselaer Polytechnic Institute, Troy, NY, 1994.

[60] Dobry R, Taboada VM. Possible lessons from VELACS Model no. 2 results. In: Arulanandan K, Scott RF, editors. Proceedings of the International Conference on the Verification of Numerical Procedures for the Analysis of Soil Liquefaction Problems, vol. 2. Rotterdam: Balkema, 1994. p. 1341–52.

[61] Hushmand B, Crouse CB, Scott RF. Centrifuge liquefaction tests in a laminar box. Geotechnique 1988;38(2):253–62.

[62] Van Laak P, Taboada VM, Dobry R, Elgamal AW. Earthquake centrifuge modeling using a laminar box. In: Ebelhar RJ, Drnevich VP, Kutter BL, editors. Dynamic geotechnical testing. ASTM STP 1213, vol. II. Philadelphia, PA: ASTM, 1994.

[63] Tan TS, Scott RF. Centrifuge scaling considerations for fluid-particle systems. Geotechnique 1985;35(4):461–70.

[64] Elgamal AW, Zeghal M, Taboada VM, Dobry R. Analysis of site liquefaction and lateral spreading using centrifuge model tests. Soils Found 1996;36(2):111–21.

[65] Elgamal AW, Zeghal M, Parra E. Liquefaction of reclaimed island in Kobe. Jpn J Geotech Eng, ASCE 1996;122(1):39–49.